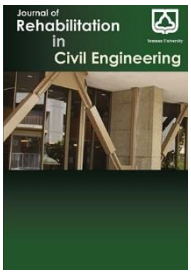

journal homepage: http://civiljournal.semnan.ac.ir/

Edged Inverted Folded Plate Shell Strip Foundation Bearing Capacity Comparison with Strip Footing on Sandy Soil

Keyhan Sajedi[1], Jafar Bolouri Bazaz[2*]

1. Ph.D. Candidate, Civil Engineering Department, Ferdowsi University of Mashhad, Mashhad, Iran.
2. Associate Professor, Civil Engineering Department, Ferdowsi University of Mashhad, Mashhad, Iran.
*Corresponding author: Bolouri@um.ac.ir

ARTICLE INFO

Article history:
Received: 02 April 2021
Revised: 05 November 2021
Accepted: 08 November 2021

Keywords:
Folded plate shell;
Elastic perfectly plastic
Analysis;
Stress;
Settlement;
Bearing capacity.

ABSTRACT

Using shell foundations as well as their benefits in the case of improved bearing capacity is investigated these days, especially strip folded shape. Because of more contact in soil, these type of shells have more bearing capacity than shallow foundations. In this research the behaviour of Strip Inverted Folded Plate Shell Foundation is studied on sandy soil. The elastic perfectly plastic numerical analyses and experimental tests are analysed and compared with shallow foundation. The effect of adding edge, variation in width and shell angle are considered. More than 45 geometrical shells models have been selected for research and the results are compared with common strip foundation in same width. Digital stress transducers are used for integrity of stresses and numerical model verification. The results indicate that adding edge with the same width and decreasing the B/D ratio in shell strip foundation improves the bearing capacity. Also when an edge on the toe of the foundation equivalent to the embedment depth is used the bearing capacity is improved in the range of 3-50%. Variation in shell angle with the same width results in increasing the bearing capacity up to two times. Finally, it is recommended to use a shell strip foundation with of 45º to 60º and with an edge equal to embedment depth.

1. Introduction

The bearing capacity of shell strip foundations depends on the further existent friction in the base level. As compared to flat foundations, shell foundations have a larger area of contact with the soil due to geometry. Therefore, shell footings are capable of carrying a larger load through more contact with the soil. Round beams and edges are the

How to cite this article:
Sajedi, K., Bolouri Bazzaz, J. (2022). Edged Inverted Folded Plate Shell Strip Foundation Bearing Capacity Comparison with strip footing on Sandy Soil. Journal of Rehabilitation in Civil Engineering, 10(3), 121-140
https://doi.org/10.22075/JRCE.2021.22649.1495

important characteristics of shells in bearing capacity. It is well known that shell foundations are cost-effective when heavy loads are to be sustained by weak, mud or saturated soils. Such situations demand large-sized foundations due to the low bearing capacity. If bending members such as slabs and beams are used, the bending moments and shears in them will be large and the required sections will also be large. Shells structure which act mostly in tension or compression will be more efficient and economical in such situations. Even in smaller foundations, the amount of materials that is necessary for a shell to carry a load will be considerably less than that required for bending members such as beams and slabs. However, the labour involved in shell construction (in forming the shell surface, fabricating steel, supervision, etc.) will be more than that is necessary in conventional type of foundations. Thus, in such special situations, one can consider the use of shells as foundations [1]. Several theoretical and experimental investigations have been carried out to investigate some characteristics of shell foundation footings, such as stress, strain, and deformation. Finite elements methods, finite difference processes, and analytic schemes have been used to analyze the behaviour of shell foundations [1].

Many investigations have focused on shell foundations with different geometrical shapes. In 2006, Alraziqi [2] indicated that utilizing the inverted shells in a foundation would help increase the bearing capacity. He studied the bearing capacity of single-shell foundations, experimentally and numerically. He found that adding edges and circumferential beams to shells improve the bearing capacity. Abdel-Rahman and Hanna [3] performed an experimental investigation to study the ultimate bearing capacity of triangular shell strip footings on sand. Their results indicated that triangular shell footings provide a higher bearing capacity and produce less settlement under the same loading conditions. They used four shell types of footings with peak angle varying from 60 to 180 degrees. They studied the geotechnical effects of the conical and folded shells on sand with different levels of density as well. These researchers investigated the influence of shell configuration and embedment depth on the ultimate bearing capacity and settlement. They ultimately concluded that increasing the depth leads to an increase in the foundation bearing capacity [4].

Kurian et al. [5] studied the effect of loading type with eccentricity on different forms of the shell on frictional and cohesive soils. These foundations were spherical, conical, and parabolic. They used both experimental and numerical strategies. They considered elastic perfectly plastic behavior and Mohr-Coulomb theory in their analysis. They found a decrease in foundation bearing capacity caused by the type of loading considering off-axes case. Bujang et al. [6] performed an elastic nonlinear analysis for single and strip footings in sandy soil. They numerically studied the effect of adding edge beams at the bottom of the shell footings and found that this approach leads to an increase in load-carrying capacity of the footing. Esmaeeli and Hatef [7] determined the ultimate load capacities of the conical and pyramidal shell foundations on plain and reinforced sand. Experimental tests were compared with numerical analysis. They found that an increase in the height of the foundation and

using reinforced sand help improve the bearing capacity.

Shaligram [8] investigated the influence of a geotextile layer level on the load-carrying capacity of triangular shell strip footings resting on reinforced layered sand. He concluded that a triangular shell footing with a peak angle of 60º results in the highest ultimate load-carrying capacity. Also, placing geotextiles below the footing and in Prandtl's radial shear zone has the highest influence on increase in load bearing capacity. Rinaldi [9] studied the function of both inverted and upright shell footings in sand while using experimental and numerical analyses. He investigated the effect of using fiberglass reinforced plastic (FRP) in a shell footing and the influence of shell angle and thickness in both cases as well. The results indicated that utilization of FRP increases the load-carrying capacity of the footing resting on sand by 42–45%, and the rupture surfaces were shown to go deeper with an increase in both shell angle and thickness. The inverted triangular shell footing load-carrying capacity was found to be 28% higher than the conventional footing. He also concluded that an increase in the shell angle and thickness of the inverted shell footing leads to higher load-carrying capacity. Stress concentration in an inverted-shaped footing is far less than in an upright case.

Azzam et al. [10] considered the ultimate load capacities of shell foundations on unreinforced and reinforced sand. The study indicated that the ultimate load capacity of shell footing on reinforced subgrade is 2.8 times higher than on unreinforced subgrade and that the load-settlement curves were significantly modified. The shell foundation over reinforced subgrade can be considered a good method to increase the bearing capacity. Also, the rupture surface of a shell-reinforced system was significantly deeper than both normal footing and shell footing without reinforcement. Al-Azzawi [11] considered the effect of adding beam edge and shell angle. He compared the experimental and numerical analysis. The results showed that decreasing the top angle and adding an edge beam led to improved bearing capacity. The comparison had only 10–14% difference in numerical and experimental cases. Sajedi et al. [12] considered the elasto-plastic behavior of strip-folded plate shell foundation in numerical analysis. They verified the observation in the Rinaldi investigation. They found that perfectly elastic plastic models had results close to Rinaldi's investigation instead of hardening model case. Moreover, the maximum shear and bending stress occur on symmetrical axial of the shell models. In another investigation, Sajedi et al. [13] considered the behavior of four types of strip-folded plate shell on dense and loose sand. They used experimental test and numerical models in their investigation. They found that both numerical and experimental analyses have similar results. They also recommended using a typical four-sided shell foundation to achieve higher bearing capacity.

Based on previous investigations, 45 experimental tests based on geometric sections were used to understand the bearing capacity of the inverted strip-folded shell strip foundations on sandy soil. Shells were designed with or without an edge and with various shell angles and widths under uniform load. Numerical analyses and digital sensors have been used for verification and analysis.

2. Strip models and digital sensors

2.1. Strip **mo**del

Based on executive aspect and previous research, the foundation shown in Figure 1 was selected for this investigation. 45 models with various widths, angles, and edges designed for experimental tests.

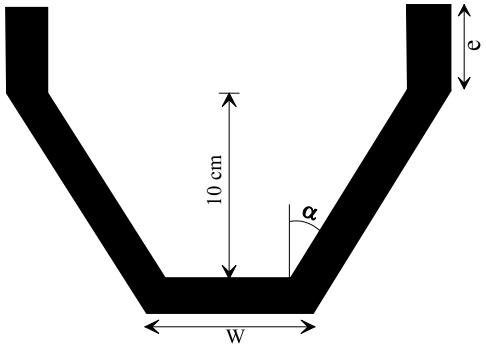

Fig. 1. Geometric shape of inverted shell strip foundation.

Embedment depths (D_f) were assumed to equal 10cm for all models without edge. The foundations designed with middle width (w) of 10, 15, and 20 cm; shell angle (□) of 0º, 30º, 45º, 60º, and 90º; top edge (e) of 5, 10 cm; and no edge. The results were compared with shallow strip foundation (foundation type E). The foundations were made of steel plates of 10cm thickness connected via continuous welding and showing no deflection during loading. Figures 2 and 3 show samples of selected models of shell strip foundations.

Fig. 2. A sample of shell strip foundation model with digital pressure transducers.

Fig. 3. Various shapes of designed shell strip foundation.

2.2. Installed digital sensors

Four kinds of sensors have been used in this research:

- Load cell (connected to the hydraulic jack).
- Vertical displacement sensor.
- Six digital pressure transducer sensors to measure contact stress of foundation and stress in soil depth.
- A 16-channel monitoring box together with data acquisition system for data recording.

2.3. Shell formation

Five categories of experiments were conducted, identified as A, B, C, D, and E. Each test indicates with a special denomination, namely (Alphabet-W*- D_f *-e). Alphabet characters A, B, C, and D show the foundation name with shell angle of 30º, 45º, 60º, and 0º, respectively; and character E illustrates a common shallow strip foundation. Character W* in denomination shows the middle width of the foundation. The middle width (W) is equal to 10, 15, and 20 cm. The width of the foundation contains middle width and side width that is related to the embedment depth and shell angle. Embedment depth was shown by D_f and the value concerning to the edge is equal to 10, 15, and 20 cm. The last character of denomination (e) states the value of the edge on top of the shell foundation. It is equal to zero, 5, and 10cm. For example, the symbol C-W10-D_f15-0 means the foundation has a

shell angle of 60º, middle width of 10 cm, embedment depth of 15 cm, and no edge. The properties of the models are given in Table 1, in which the unit of length, area, and angle are centimetre, square centimetre, and degree respectively. B/D is the ratio of total horizontal width to embedment depth. A_{XY} is the effective area obtained from the multiple of total width and width of tank (40 cm), which is used to calculate effective vertical stress.

Table 1. Properties of inverted shell strip foundation model.

No	model	Shell angle	Embedment depth (D_f)	Edge (e)	Total width (B)	Middle width (W)	B/D ratio	A_{XY}
1	A-W10-Df10-0	30	10	0	21.5	10	2.15	860
2	A-W10-Df15-5	30	15	5	21.5	10	1.4	860
3	A-W10-Df20-10	30	20	10	21.5	10	1.1	860
4	A-W15-Df10-0	30	10	0	26.5	15	2.65	1060
5	A-W15-Df15-5	30	15	5	26.5	15	1.8	1060
6	A-W15-Df20-10	30	20	10	26.5	15	1.3	1060
7	A-W20-Df10-0	30	10	0	31.5	20	3.15	1260
8	A-W20-Df15-5	30	15	5	31.5	20	2.1	1260
9	A-W20-Df20-10	30	20	10	31.5	20	1.6	1260
10	B-W10-Df10-0	45	10	0	30	10	3	1200
11	B-W10-Df15-5	45	15	5	30	10	2	1200
12	B-W10-Df20-10	45	20	10	30	10	1.5	1200
13	B-W15-Df10-0	45	10	0	35	15	3.5	1400
14	B-W15-Df15-5	45	15	5	35	15	2.3	1400
15	B-W15-Df20-10	45	20	10	35	15	1.75	1400
16	B-W20-Df10-0	45	10	0	40	20	4	1600
17	B-W20-Df15-5	45	15	5	40	20	2.6	1600
18	B-W20-Df20-10	45	20	10	40	20	2	1600
19	C-W10-Df10-0	60	10	0	45	10	4.5	1800
20	C-W10-Df15-5	60	15	5	45	10	3	1800
21	C-W10-Df20-10	60	20	10	45	10	2.25	1800
22	C-W15-Df10-0	60	10	0	50	15	5	2000
23	C-W15-Df15-5	60	15	5	50	15	3.3	2000
24	C-W15-Df20-10	60	20	10	50	15	2.5	2000
25	C-W20-Df10-0	60	10	0	55	20	5.5	2200
26	C-W20-Df15-5	60	15	5	55	20	3.7	2200
27	C-W20-Df20-10	60	20	10	55	20	2.75	2200
28	D-W10-Df10-0	90	10	0	10	10	1	400
29	D-W10-Df15-5	0	15	5	10	10	0.65	400
30	D-W10-Df20-10	0	20	10	10	10	0.5	400
31	D-W15-Df10-0	0	10	0	15	15	1.5	600
32	D-W15-Df15-5	0	15	5	15	15	1	600
33	D-W15-Df20-10	0	20	10	15	15	0.75	600
34	D-W20-Df10-0	0	10	0	20	20	2	800
35	D-W20-Df15-5	0	15	5	20	20	1.35	800
36	D-W20-Df20-10	0	20	10	20	20	1	800
37	E-W10-Df10-0	90	10	0	10	10	1	400
38	E-W15-Df10-0	90	10	0	15	15	1.5	600
39	E-W20-Df10-0	90	10	0	20	20	2	800
40	E-W25-Df10-0	90	10	0	25	25	2.5	1000
41	E-W30-Df10-0	90	10	0	30	30	3	1200
42	E-W35-Df10-0	90	10	0	35	35	3.5	1400
43	E-W40-Df10-0	90	10	0	40	40	4	1600
44	E-W45-Df10-0	90	10	0	45	45	4.5	1800
45	E-W50-Df10-0	90	10	0	50	50	5	2000

2.4. Model scaling

Physical modelling is divided into two categories: small-scale and full-scale models. Full-scale physical modelling can simulate the real site conditions such as ground conditions, pressures, and stress levels. However, due to the difficulty of preparing the conditions for this type of modelling as well as its high cost, theory of similarity and scaling law used for small-scale physical models. Replacement of a prototype with a plate N times smaller in dimensions results in an ultimate bearing capacity N times smaller than that of the prototype. In this study, a small-scale model with a ratio of 5 times smaller than the ratio of a hypothesized prototype was built (shown in figure 3). As the stress levels are low in a small-scale modelling, the stress-strain behaviour of prototype was considered for the model, too. In addition, the scaling factors were assumed in this study. Table 2 shows the applied theory of scaling law offered by Wood [14]. Jafarian et al. [15] applied the Vargas-Monge [16] data and the brittleness index concept proposed by Bishop et al. [17] to account for the correlation of relative density and effective stress level between the model and the prototype scales. For the northern sand of Iran, they decreased the relative density (Dr) of the sand about 20% in the model scale in order to compensate for the 10 times smaller effective stress level, leading to more dilatant behaviour in the model test. This type of scaling has been commonly used for the 1g model tests [15]. Therefore, in this study, the medium state of the Firuzkooh sand in the 1g box was achieved with Dr = 60% corresponding to Dr = 80% in the prototype scale using the adopted scaling factor (N=10).

Table 2. Scaling factor used to convert the parameters to prototype units [14].

Parameters	Scale factor (prototype/model)
Length	N
Displacement	N
Mass density	1
Stress and pressure	$N^{2-\propto^*}$
Stiffness	$N^{\propto}$

*: for sand $\propto$ is equal 0.5

3. Soil characteristics and test setup

In order to study the behaviour of shell foundation an experimental setup was designed to perform a testing program. As s sand reservoir, a cubical tank with rigid steel frame and glass panels with 2000 mm, 1700 mm and 400 mm in length, depth, and width, respectively was designed and made (Figure 4). The tank is large enough to prevent boundary effects. The frame has high rigidity to bear no significant deformation due to the applied loads. The glass panel of the tank facilities to observe soil layer deformation. A hydraulic jack with one millimeter in a minute speed was employed to apply vertical load to the shell strip (Figure 5).

Fig. 4. A general photo of soil reservoir with soil pressure transducer and data acquisition.

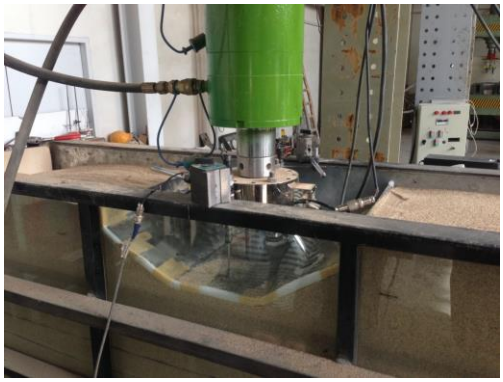

Fig. 5. The designed apparatus under laoding.

In order to measure the soil pressure beneath the foundation and in depth, nine pressure transducer, three of which connected to the strip (Figure 2) and the rest installed in different levels inside the soil mass (Figure 4). The pressure transducers were employed in this research to measure the normal stress as shown in Figure 6. Diameter of transducers are 5 cm and work with 24 voltages. The output of this type of transducer is 4 to 20 milliampere. Before installation of transducers, they were calibrated with the aid of various water pressure supplied from triaxial apparatus. Shown in Figure 6 is the variations of pressure (in terms of mPa) versus sensor output (in terms of milliampere). Also a data acquisition system with 16 channel were employed to record output data.

"Firoozkooh sand" from the North of Iran was used for experimental and numerical models. Physical and mechanical parameters and soil gradation graph of this type of sand are presented in Table 3 and Figure 7. A new raining system, which has been designed and developed at the soil mechanic research center of Ferdowsi University of Mashhad was employed to fill the tank reservoir by Abdollahi et. al. [18]. This system, which has been fully described in detail elsewhere is able to create a sand bed with specified density. The adjustment of height and raining curtain facilitates to create sand layers with identical and desired density. Here the density of prepared sand reservoir was 80%±1 corresponding to dry density of 15.1 kN/m^3.

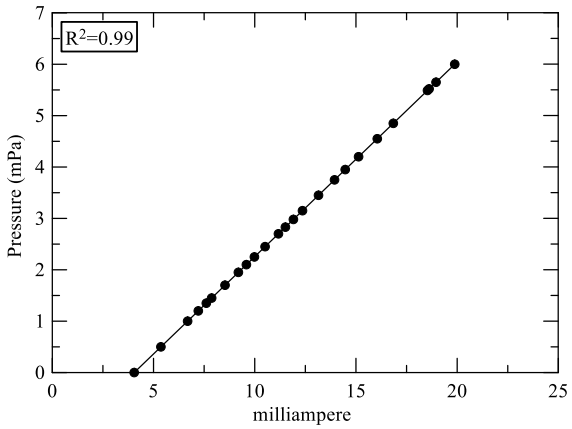

Fig. 6. Calibration of pressure transducers.

Table 3. Properties of Firouzkooh sand.

Parameters	magnitude	Unit
Moisture content	1%	-
G_s	2.71	-
Dry unit weight	15.13	kN/m^3
Prosperity	1.048	-
Cohesion coefficient	0.001	kN/m^2
Internal friction angle	32	Degrees
Dilation angle	2	Degrees
Poisson ratio	0.3	-
Young modulus	30	MPa
Relative density	80%	-
e_{max}	1.04	-
e_{min}	0.7	-
Soil pattern	Mohr colomb	

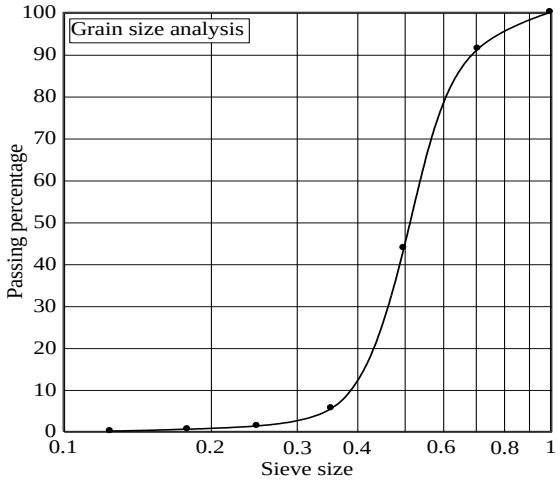

Fig. 7. Sandy soil gradation.

4. Finite element model

The finite element method was used for the numerical analysis, employing PLAXIS software. Mohr-Coulomb elastoplastic model, as a behavioral model has been employed for stress-strain analysis.

4.1. Properties of materials

The properties of Materials, used in the numerical modelling have been extracted from laboratory experiments of soil mechanic performed on Firouzkouh sand with the same relative density as listed in table 4. The main and the most affective parameters of the Mohr-Coulomb model is elastic modulus (E), which has been determined experimentally using triaxial test.

4.2. Numerical model

Based on the experimental setup, the plane strain state was assumed for the problem when employing PLAXIS software. The soil media was meshed by using 15-node triangular elements. A very fine size of mesh was utilized for the contact area of the foundation and soil, fine size for the area close to the foundation, and medium size for the other regions of the soil mass. The arch-length method was used for nonlinear analysis, and the load was applied in 250 increments. In nonlinear hardening analysis using PLAXIS, displacement control versus increasing the incremental load was obtained through the arc length method. The dimension of the boundary model is considered to be 10 times the foundation width from around and 8 times the foundation depth from below. Boundary conditions in bottom of the model are considered with no displacement, while on the left and right sides, the displacement is free in the vertical direction but fixed in the horizontal direction. The foundation is assumed to behave rigidly. The sandy soil is analyzed in perfectly elastic-plastic state. Figure 8 depicts the A-W10-Df10-0 model mesh. The Mohr-Coulomb model was also employed for elastic-plastic behaviour of the soil. Because the foundation is symmetric, only half of the model is included. The scale of the numerical model is the same as experimental set up. The deformation of the C-W10-Df10-5 model has been shown in Figure 9.

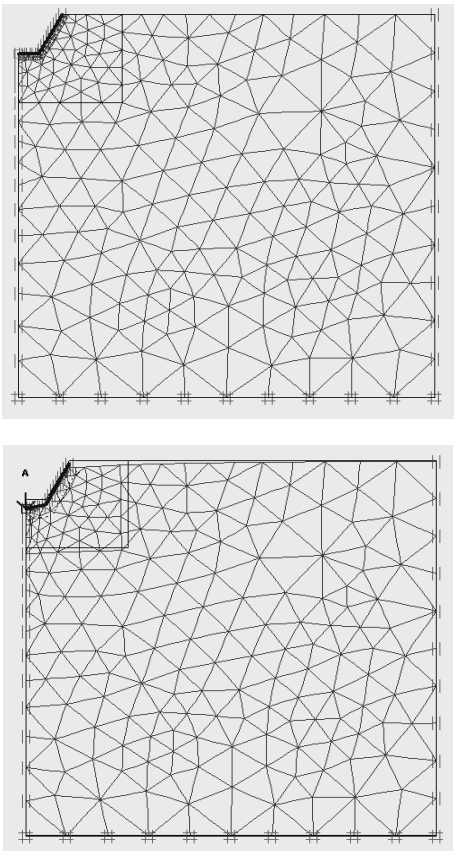

Fig. 8. Mesh model of A-W10-Df10-0 Before and After deformation.

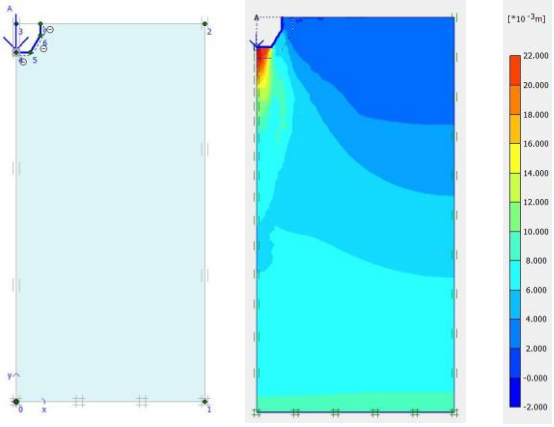

Fig. 9. Load modelling and deformation of A-W10-Df10-5.

The extension of the plastic region for model C-W10-Df10-0 at different steps of loading (q=5, 25, 50, 100, 130 and 160 kN/m) is shown in Figure 11. In the elastic perfectly plastic behavior, the shallow soils have tensile local failures. With increasing the stress beneath the foundation, the plastic region near the foundation becomes deeper and the second wedge will be formed under the first wedge. In the elastic perfectly plastic soil, the depth of the failure wedge, H, in the numerical analysis is more than what recommended by Rinaldi's relation (Eq. 3) [9]. This depth approaches up to 3 times of the embedded depth of the foundation. The assumption in Rinald`s method is based on a uniform contact normal stress and a linear failure wedge (figure 10). Consequently, Rinaldi`s failure wedge depth develops lower than the real value. Ultimate bearing capacity solution was only theoretically corrected, if the system was statically and kinematically admissible. Static equilibriums were satisfied as all limit equations are satisfied $\left(\sum F_x = 0. \sum F_y = 0. \sum M = 0\right)$ i.e. the shear stress on a soil element was equal to the shearing resistance of the sandy soil along the rupture surface. The conditions of kinematics were fulfilled if the movement and displacement of soil elements along the rupture plane were feasible.

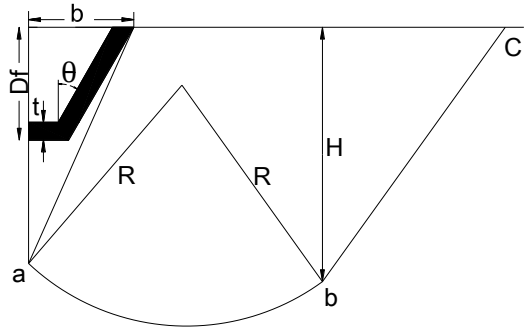

Fig. 10. Rupture surfaces of inverted shell strip foundation in Rinaldi's analytical model [9].

The simplified failure surface is used for determining bearing capacity coefficients, $\left(N_c . N_q . N_\gamma\right)$ and consequently, ultimate bearing capacity(q_u). In Rianldi's theoretical relation, θ is the shell angle between the shell surface and the vertical line. α is the failure angle which is dependent on the shell ratio

(*SR*), and the angle of shearing resistance (Φ). The following relations are available for calculating α and *SR* values [9]:

$$\alpha = \Phi + (SR - 2)\left(\frac{\pi}{4} - \frac{2\Phi}{3}\right) \quad (1)$$

where,

$$SR = \frac{\pi + 2\theta}{\pi} \quad (2)$$

SR is the shell ratio that specifies the effect of shell strip shape at the failure angle (α). There are three limits for *SR*. For the case of flat foundation *SR*=1 (θ=0), for the piles *SR*=2 (θ=90°). For inverted shell strip foundation, the values of *SR* are between 1 and 2. These values are between 0 and 1 for upright shell foundations. Another parameter for the theoretical equation is soil failure height (*H*) that is calculated from the following relation [13]:

$$H = D_f + b\tan\alpha + R\left[\sin(\frac{\pi}{4} + \frac{\phi}{2}) - \cos(\frac{\pi}{4} + \frac{\phi}{2})\right] \quad (3)$$

In this equation, R is the circle radius, b is half of the foundation width, Φ is soil internal friction angle, and D_f is foundation depth. In Rinaldi theoretical method, the contact normal stress is assumed to be uniform. Maximum settlement occurs in the symmetry axis of the foundation. variation of maximum normal contact stress versus the applied loads, in elastic perfectly plastic analysis is shown in Figure 12. the normal contact stress in all models is non-linear and this quantity in inclined part is very lower than the horizontal part.

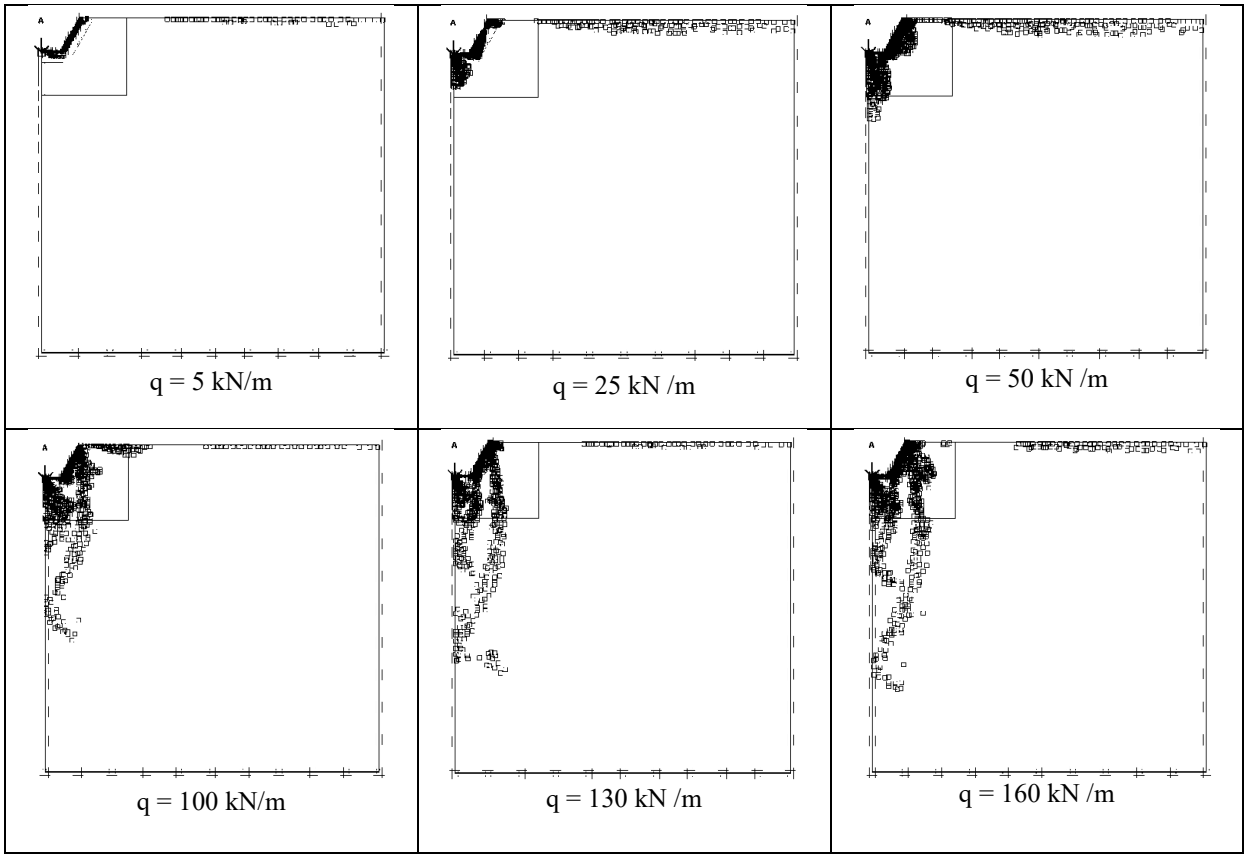

Fig. 11. Plastic region and development of a rigid wedge in model C-W10-Df10-0.

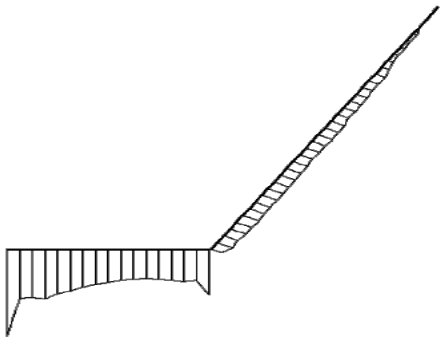

Fig. 12. Non-uniform contact normal stress in the half inverted folded shell.

4.3. Model verification

It is a common practice to compare the results gained from either FE analyses or analytical approach with real cases, field data or experimental results. This practice is well known as "back analysis" for dam projects in which the instrumentation data are compared with model outputs in both construction period and long term behaviour of dams (Bolouri Bazaz et. al. [19]). Also the soil–structure interaction for deep excavation adjacent to tall building is another example to verify the numerical modelling of excavation (Yegane et. al. [20]). The most fundamental stages in numerical modelling are specifying the appropriate geometric boundaries so that the effect of such boundaries reaches its bottommost magnitude on the results, and choosing real material specifications of model. Finally, it is worth mentioning that for the calibration of a numerical model, the outputs of model including both stress and deformation may be compared with real values derived from field or experiment data.

In the present research, the approach of considering appropriate boundaries was explained earlier, however the main parameter of Mohr-Coulomb model, i.e. Young modulus is chosen by back-analysis.

The first step of model verification is the foundation settlement of the numerical outputs and comparing with experimental results. This was achieved by substitution of various magnitudes of elastic modulus of soil from Es=20 to 70 kPa. The settlement of point 1 (shown in picture 19) was measured during loading in each sample. In experimental tests, foundations settled down around 20 millimetres under 25 to 45 kN forces. Based on the experimental curve for point 1, by selecting Es less than 30 kPa in numerical analysis, the foundations settlement is less than 15 mm settlement by the same force and during analyzing, models were collapsed. By selecting more than Es=50 kPa, more forces settled down the foundations. The best harmonization in load-settlement curve was happened in 40 kPa. Figure 13 shows the load-settlement variation by various Es in sample C-W15-Df15-5. It could be observed the most appropriate of magnitude of Young modulus is about Es= 40 kPa. Based on this value of Es the stress at different points were derived from numerical model. Normal stresses were measured in 2.5, 5, 10 and 20 mm deformation as well.

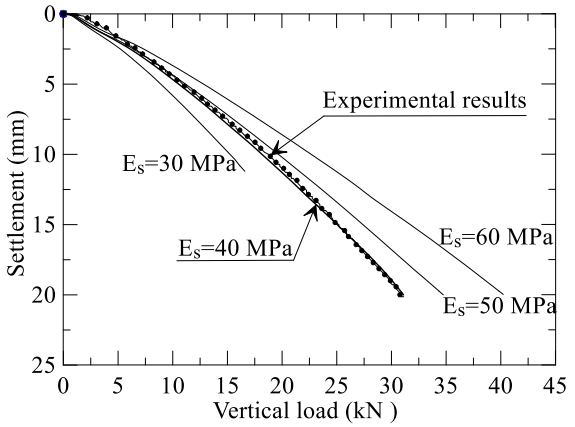

Fig. 13. load- settlement curve of C-W15-Df15-5 for point 1 for experimental test and numerical analysis.

For verification of stresses in numerical analysis, normal stress of six specified points (inside the soil tank and beneath the foundation, where the transducers were installed) and two or three points in the center and beside the shell foundation (shown in Figures 19) were taken from numerical analyses and compared with the real magnitudes of transducers data. This issue has been explained in more details in section 5.4. Figures 20 and 21 show the numerical verification with transducers response.

5. Experimental results

In this section, the ultimate bearing capacity and maximum stress of 45 various shell models are compared. The effect of the top edge and angle are considered. For instance, the load settlement curves of foundation type A are plotted and shown in Figure 14-a. The behavior of maximum vertical stress curves of soil and foundation type A are considered in Figure 14-b. Experimental and numerical analyses show that while width increases in a specified embedment, bearing capacity improves. At the same width, an increase in embedment depth causes bearing capacity to improve as well. If these parameters vary together, the character B/D can explain the variation. Four case of settlement (2.5, 5, 10 and 15 mm), have been selected for comparison of results to face the behavior of shell foundation.

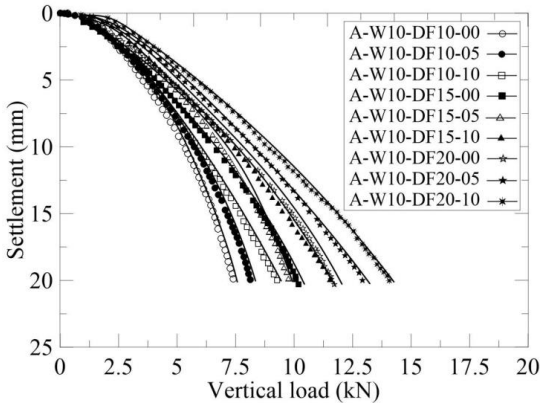

Fig. 14-a. load- settlement curve of the shell foundation type A: experimental results.

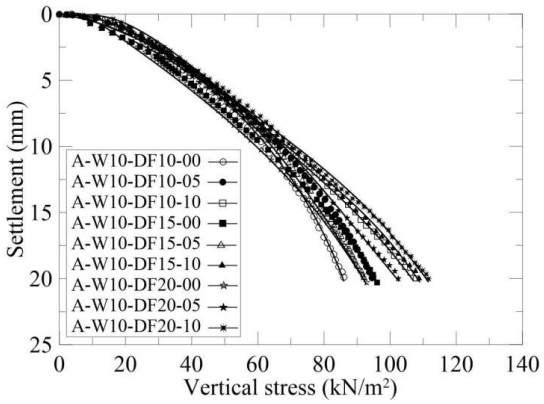

Fig. 14-b. stress- settlement curve of the shell foundation type A: experimental results.

Figure 15 shows the variation of B/D ratio and the bearing capacity in 45 various shell samples. Based on results in the same middle width, bearing capacity reduces when the B/D increases. This consequence occurred in various settlements.

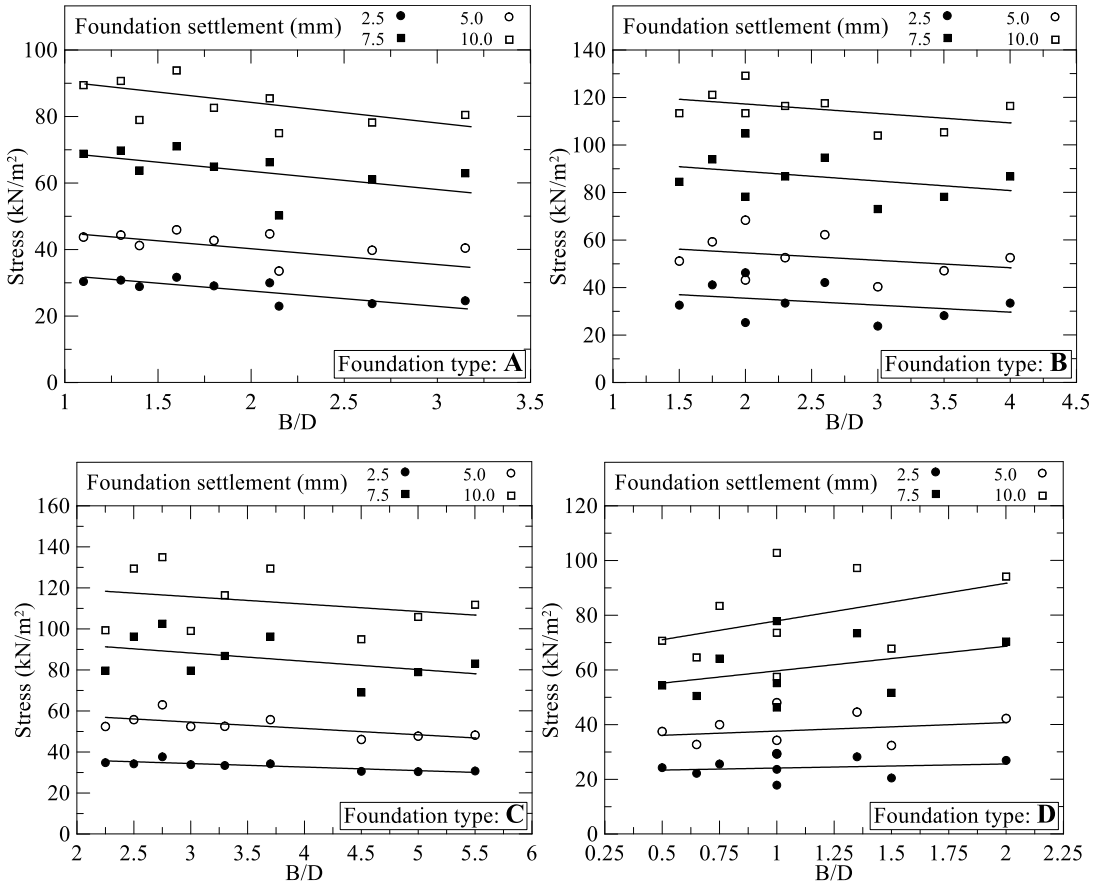

Fig. 15. variation of B/D and bearing capacity of shell foundations in different settlement.

5.1. Effect of width on bearing capacity

To demonstrate the influence of increase in width of shell foundation, Figure 16 shows that bearing capacity improves 3–25% when the middle width widens to around half of the embedment depth and 5–50% when it is equal embedment depth. Results are obtained in the same settlement (at 2.5 mm). In other settlements, the results are approximately the same. Foundation type B experienced the highest influence of change in width toward foundations A, C, and D.

5.2 Effect of shape and embedment depth on bearing capacity

Figure 17 shows the comparison of the shell's bearing capacity with the various shape configurations. In all faces, bearing capacity in a shell is more than in a shallow foundation, namely 10–40%. Moreover, bearing capacity improves 5–12% if the embedment depth increases 1.5 times and 7–25% when it rises 2 times. In the case of shape, foundation type C has the best shape in shells to achieve higher bearing capacity, whereas type D has the lowest capacity. Results show closely answers in Foundation Types B and C. So in this case, it seems that the foundations with shell angles of 45º to 60º are better options than shells with angles less than 45º.

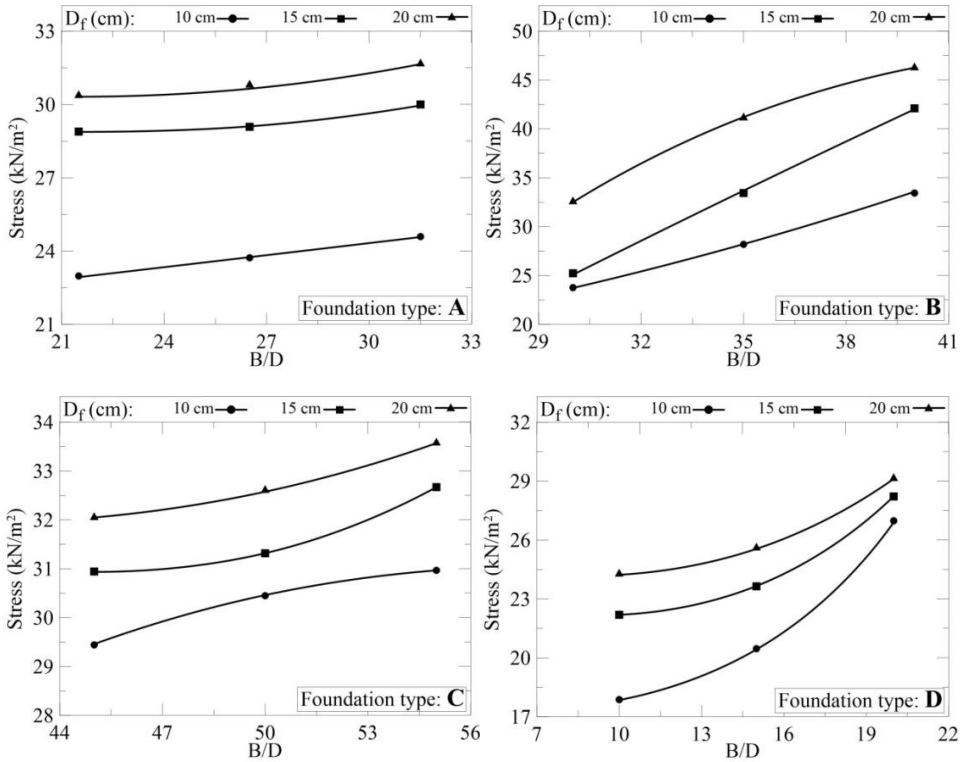

Fig. 16. effect of width on the bearing capacity of shell foundations (settlement=2.5mm).

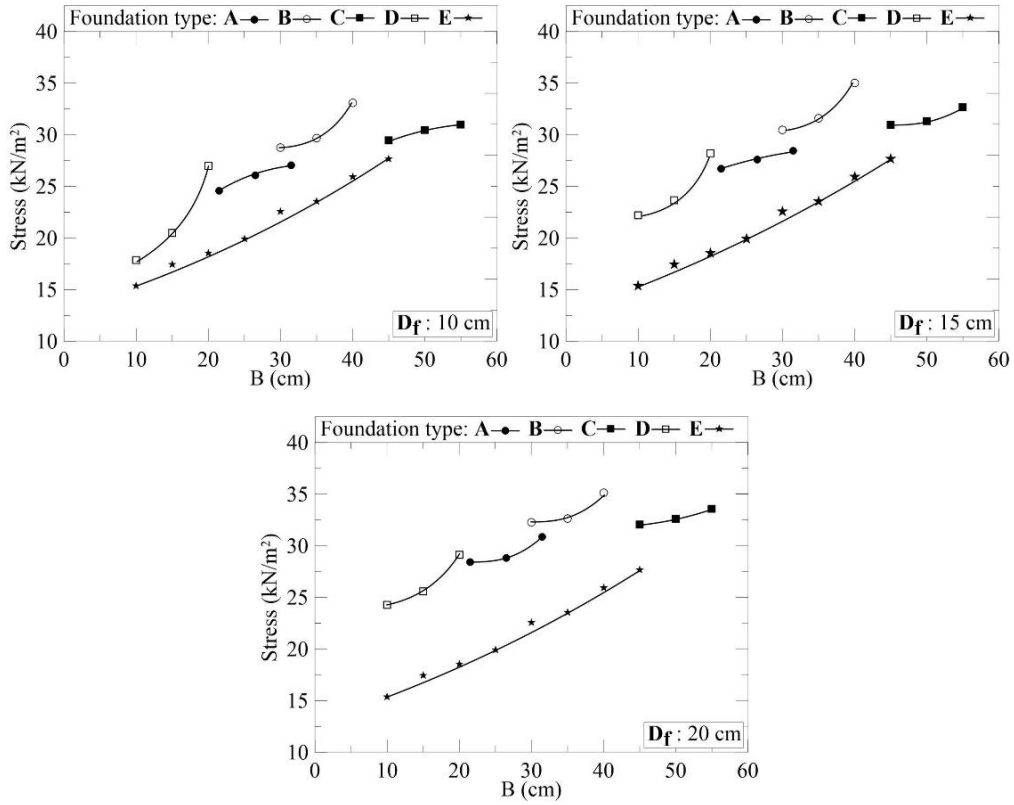

Fig. 17. bearing capacity of shells in different depth and shape.

5.3. Effect of adding edge on bearing capacity of shells

A comparison of the bearing capacity of the shell footings with the various edge configurations is shown in Figure 18. In all cases, the load carried by shell foundations with top edge is more than the footing without edge. Analysis was done on shells with edges (e) equal to embedment depth, half of that, and without edge. Results show that bearing capacity improves 3–30% when an edge equal to half of the embedment depth is added to the top of shells. The improvement is 9–50% if the edge is equal to embedment depth.

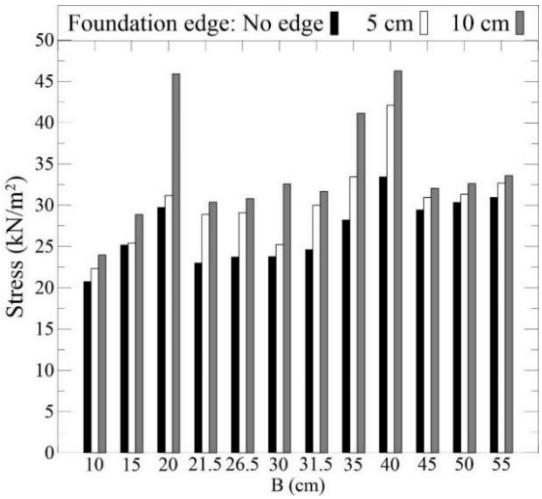

Fig. 18. effect of adding edge on the bearing capacity of shell foundations.

5.4. Stress verification

Digital stress transducer sensors were used for integrity of stresses. For verification of numerical analysis and experimental tests, digital sensors were used at four levels. One was inside the foundation, and three were inside the soil. Figure 19 shows these levels in numerical and experimental tests. They are 30, 55, and 80 cm under the foundation level. Initial stress in sensors due to soil weight is around 0.03 to 0.15 kg/cm^2. Figure 20 indicates a difference between the answers. In this Figure, a sample of settlement-stress curve is indicated for each foundation in numerical analysis and digital sensor, which is sited under the foundation.

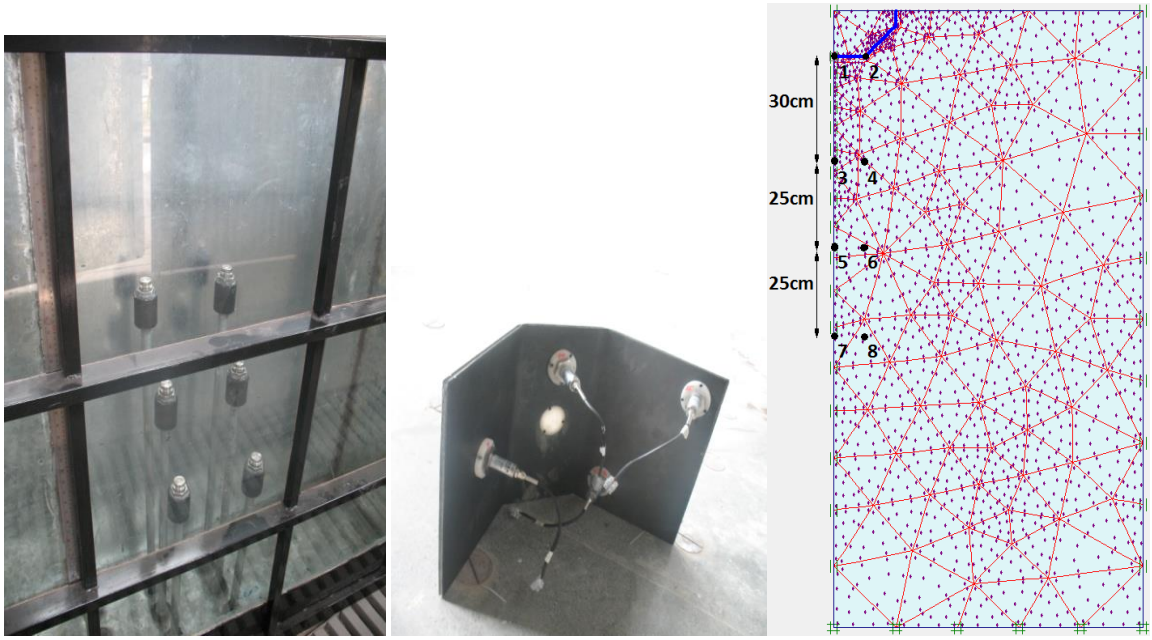

Fig. 19. digital sensors for verification in the model, tank and shell foundations.

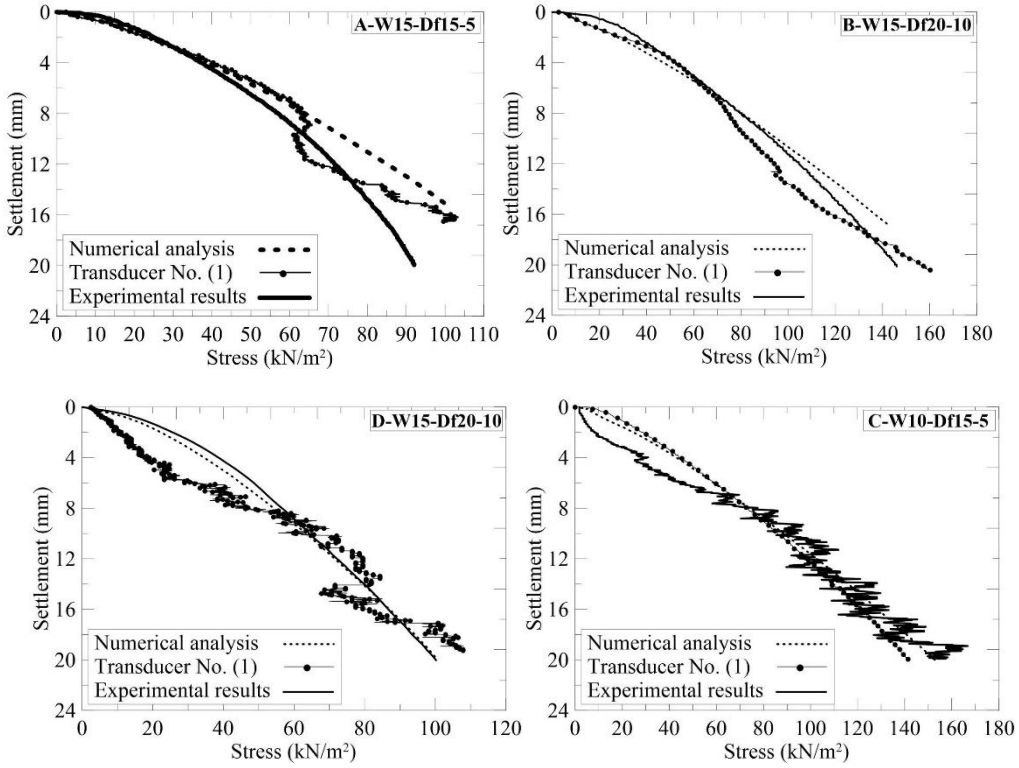

Fig. 20. stress-settlement verification in digital sensors and numerical analysis.

Moreover, stresses in the settlement of 2.5, 5, 10, and 15 mm in both experimental and numerical analyses are shown in Table 4. Based on research, 59% of data have 1–10% difference, 28% have 10–20%, and only 13% have a 20–45% difference in bearing capacity results. So we can say the experimental and numerical models have satisfied the overlapping of answers.

Table 4. comparison between experimental and numerical stresses.

Model	S=2.5mm			S=5mm			S=10mm			S=15mm		
	Exp. (Kg/cm2)	Num. (Kg/cm2)	Difference (%)	Exp. (Kg/cm2)	Num. (Kg/cm2)	Difference (%)	Exp. (Kg/cm2)	Num. (Kg/cm2)	Difference (%)	Exp. (Kg/cm2)	Num. (Kg/cm2)	Difference (%)
A-W10-Df10-0	0.23	0.25	6.44	0.34	0.42	19.30	0.51	0.69	25.57	0.63	0.87	26.98
A-W10-Df15-5	0.29	0.27	8.06	0.42	0.44	5.41	0.65	0.72	10.52	0.80	0.95	15.44
A-W10-Df20-10	0.31	0.29	6.80	0.45	0.44	0.97	0.70	0.71	1.29	0.91	0.95	4.43
A-W15-Df10-0	0.24	0.27	8.97	0.41	0.44	9.41	0.62	0.71	14.15	0.80	0.95	16.35
A-W15-Df15-5	0.30	0.28	5.34	0.44	0.45	3.40	0.66	0.76	15.41	0.84	1.02	17.14
A-W15-Df20-10	0.31	0.29	6.82	0.45	0.49	8.28	0.71	0.86	20.28	0.92	1.14	18.91
A-W20-Df10-0	0.25	0.28	9.05	0.41	0.45	9.40	0.64	0.73	14.47	0.82	0.96	14.57
A-W20-Df15-5	0.31	0.29	5.44	0.46	0.48	4.74	0.68	0.79	16.27	0.87	1.04	16.64
A-W20-Df20-10	0.32	0.31	2.56	0.47	0.49	4.29	0.72	0.78	8.30	0.96	1.15	16.80
B-W10-Df10-0	0.24	0.29	17.33	0.41	0.51	23.64	0.74	0.86	14.86	1.06	1.09	2.49
B-W10-Df15-5	0.26	0.31	17.18	0.44	0.55	25.91	0.80	0.91	13.46	1.16	1.22	5.42
B-W10-Df20-10	0.33	0.33	0.94	0.52	0.56	6.83	0.86	0.95	9.98	1.16	1.27	8.86
B-W15-Df10-0	0.29	0.30	4.96	0.48	0.54	12.59	0.80	0.92	15.21	1.07	1.20	10.86
B-W15-Df15-5	0.34	0.32	5.83	0.54	0.54	1.40	0.88	0.95	6.93	1.19	1.26	5.76
B-W15-Df20-10	0.42	0.33	26.10	0.60	0.57	5.97	0.96	0.97	1.31	1.23	1.35	8.47
B-W20-Df10-0	0.34	0.34	1.09	0.54	0.59	9.85	0.88	0.99	11.76	1.19	1.36	12.73
B-W20-Df15-5	0.43	0.36	20.27	0.63	0.60	6.22	0.97	1.03	7.20	1.20	1.40	14.22
B-W20-Df20-10	0.47	0.36	31.60	0.70	0.62	11.35	1.07	1.05	1.98	1.32	1.41	6.93
C-W10-Df10-0	0.31	0.30	3.93	0.47	0.50	5.87	0.70	0.89	26.91	0.87	1.20	27.44
C-W10-Df15-5	0.34	0.32	9.20	0.53	0.53	1.49	0.81	0.93	14.24	1.01	1.25	19.16
C-W10-Df20-10	0.35	0.33	8.49	0.53	0.56	4.89	0.81	0.93	14.95	1.01	1.28	20.76
C-W15-Df10-0	0.31	0.31	0.18	0.49	0.55	13.34	0.80	0.93	15.28	1.08	1.28	15.62
C-W15-Df15-5	0.34	0.32	6.76	0.54	0.56	4.96	0.88	0.95	7.07	1.19	1.31	9.72
C-W15-Df20-10	0.35	0.33	5.04	0.57	0.58	1.79	0.98	1.01	2.74	1.32	1.44	8.51
C-W20-Df10-0	0.31	0.32	0.67	0.49	0.56	14.40	0.85	0.98	15.34	1.14	1.34	14.97
C-W20-Df15-5	0.35	0.33	4.82	0.57	0.57	0.14	0.98	1.02	3.52	1.32	1.41	6.27
C-W20-Df20-10	0.38	0.34	12.24	0.64	0.62	4.10	1.04	1.14	8.92	1.43	1.46	2.36
D-W10-Df10-0	0.21	0.18	16.13	0.30	0.30	0.46	0.46	0.47	1.81	0.61	0.59	3.87
D-W10-Df15-5	0.23	0.23	0.61	0.33	0.33	0.35	0.50	0.51	3.44	0.61	0.66	6.62
D-W10-Df20-10	0.24	0.25	1.26	0.36	0.38	7.18	0.53	0.55	3.74	0.66	0.72	8.46
D-W15-Df10-0	0.26	0.21	23.12	0.37	0.33	9.86	0.56	0.53	6.45	0.74	0.69	6.95
D-W15-Df15-5	0.26	0.24	7.47	0.39	0.35	10.66	0.65	0.56	13.01	0.87	0.75	15.59
D-W15-Df20-10	0.29	0.26	12.82	0.45	0.41	9.73	0.65	0.65	0.06	0.85	0.85	0.07
D-W20-Df10-0	0.31	0.28	13.81	0.46	0.43	7.27	0.71	0.72	0.30	0.94	0.96	2.16
D-W20-Df15-5	0.31	0.29	6.98	0.48	0.45	4.76	0.81	0.75	7.65	1.17	0.99	18.51
D-W20-Df20-10	0.47	0.30	36.52	0.72	0.49	31.57	1.17	0.79	32.02	1.53	1.05	31.71
E-W10-Df10-0	0.16	0.29	45.36	0.23	0.43	46.22	0.36	0.66	45.52	0.47	0.82	42.87
E-W15-Df10-0	0.18	0.20	12.93	0.26	0.39	33.45	0.40	0.57	30.06	0.52	0.74	29.49
E-W20-Df10-0	0.19	0.22	13.41	0.27	0.35	29.06	0.42	0.55	23.52	0.55	0.73	25.49
E-W25-Df10-0	0.20	0.17	16.08	0.30	0.30	1.95	0.46	0.47	2.03	0.61	0.64	5.12
E-W30-Df10-0	0.23	0.19	21.78	0.33	0.26	19.98	0.49	0.43	11.23	0.65	0.58	11.42
E-W35-Df10-0	0.24	0.15	37.80	0.34	0.25	27.06	0.47	0.42	11.25	0.62	0.57	8.23
E-W40-Df10-0	0.26	0.17	35.06	0.40	0.32	20.28	0.53	0.52	2.43	0.69	0.71	2.66
E-W50-Df10-0	0.28	0.19	32.83	0.42	0.33	16.47	0.64	0.56	12.33	0.85	0.79	7.38

Figure 21 shows the verification of digital data received from the sensors and the ultimate stress from numerical analysis. Transducer sensors 1 and 2 settled just under the foundation. Transducer 3 and 4 settled 30 cm under the foundation, Transducer 5 and 6 settled 55 cm under the foundation and numbers 7 and 8 settled 80 cm under the foundation. As the foundation sizes are small, the results of corner and central sensors in each level are the same. For instance, data of sample B-W15-Df20-10 are shown in Table 5 and figure 20. In each settlement, the average of difference is less than 10%.

Table 5. Comparison between experimental and numerical stresses in each level for B-W15-Df20-10.

	S=2.5mm			S=5mm			S=10mm			S=15mm		
stress	difference	Num. (kg/cm^2)	Exp. (kg/cm^2)	difference	Num. (kg/cm^2)	Exp. (Kg/cm2)	difference	Num. (kg/cm^2)	Exp. (kg/cm^2)	difference	Num. (kg/cm^2)	Exp. (kg/cm^2)
Stress in point 1&2	10.5	0.34	0.38	3.40	0.57	0.59	11.8	0.96	0.846	15.6	1.34	**1.13**
Stress in point 3&4	6	0.154	0.164	0	0.225	0.226	5	0.346	0.329	2	0.451	**0.46**
Stress in point 5&6	16	0.15	0.126	22	0.185	0.226	25	0.245	0.329	33	0.35	**0.46**
Stress in point 7&8	7.5	0.172	0.186	1	0.205	0.207	2.4	0.25	0.244	5	0.305	**0.29**

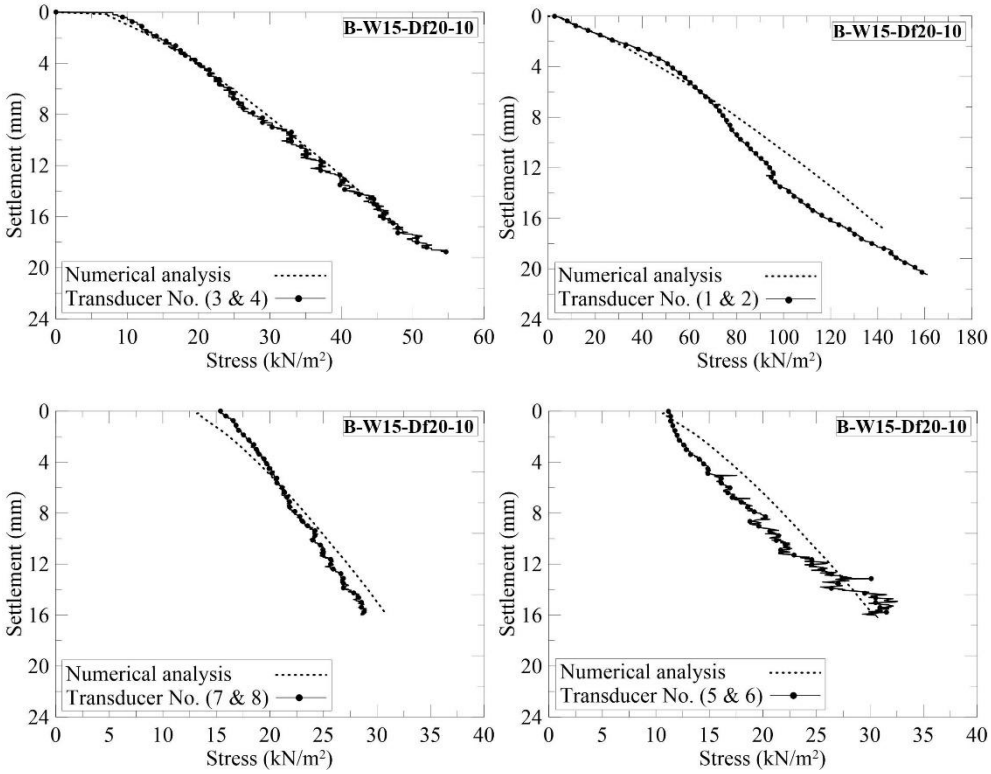

Fig. 21. stress-settlement verification in digital transducers and numerical analysis for B-W15-Df20-10 in different levels.

6. Conclusion and discussion

The stress-settlement behavior of shell footings was investigated and compared to their flat counterparts. Finite element analysis showed that the normal contact stress in all models is non-linear and its magnitude in the inclined part is much lower than the horizontal part. With increasing the stress beneath the foundation, the plastic region near the foundation becomes deeper and the second wedge will be formed under the first wedge. In the elastic perfectly plastic soil, the depth of the failure wedge, H, in the numerical analysis is more than what recommended by Rinaldi's relation [9]. This depth approaches up to 3 times of the embedded depth of the foundation. Based on the experimental and numerical investigations of four shell foundation models and shallow foundation, further existing friction in the base level and larger area of contact with the soil due to geometry cause the ultimate capacities of shell strip foundations to be 10–40% higher than those of their flat counterparts with the same plan dimensions and embedment depth. Some parameters, such as shape, width, depth, and edge on toe, are effective in improving the behavior of shell foundations. The edge on the toe of the inverted shell strip foundations help to improve bearing capacity because of the increased friction and deeper installation. Bearing capacity is improved 3–50% when an edge equal to embedment depth is used on the toe of the foundation. Non-dimensional settlement factor (B/D) was used to examine the behavior of shell foundations. The results deduced from the present investigation reveal that bearing capacity is reduced with an increase in B/D ratio. Digital stress control transducer sensors used for tests. Results showed that perfectly plastic numerical analysis have satisfied the overlapping of answers instead of experimental efforts. 87% of data have 1–25% difference.

In the case of width of shell foundation, bearing capacity increases when the middle width increases. We strongly advise using a middle width equal to the depth of the foundation to achieve 5–50% more stress capacity. Also, as for the shape, this research recommends using a shell angle of 45º to 60º instead of less than 45º to gain higher bearing capacity.

REFERENCES

[1] Kurian, N. P., (2006). "Shell foundations", Alpha Science International Ltd., India.

[2] Alraziqi, Adel Ahmed, (2006). "Geotechnical behaviour of shell footings", Ph.D. Thesis, University Putra Malaysia.

[3] Abdel-Rahman, M., and Hanna, A.M., (1990). "Ultimate Bearing Capacity of Triangular Shell Footings on Sand", Journal of Geotechnical Engineering, ASCE, Vol. 116, No. 12, pp. 1851-1863.

[4] Hanna, A.M., and Abdel-Rahman M., (1998). "Experimental investigation on shell foundations on dry sand", Canadian Geotechnical Journal, No. 35, pp. 828-846.

[5] Kurian, N.P., and Jayakrishna, Devaki, V.M., (2005). "Analytical studies on the geotechnical performance of shell foundations", Canadian Geotechnical Journal, No. 42, pp.562–573.

[6] Bujang B.K.H., and Thamer A.M., (2006). "Finite Element Study Using FE Code (PLAXIS) on the Geotechnical Behaviour of Shell Footing". Journal of Computer Science, Vol.2, No.1, pp. 104-108.

[7] Esmaili, D., and Hataf N., (2008). "Experimental and Numerical Investigation of Ultimate Bearing Capacity of Shell Foundations on Reinforced and Unreinforced Sand", Iranian Journal of Science and Technology, Vol. 32, No. B5.

[8] Shaligram P.S., (2011). "Behavior of Triangular Shell Strip Footing On Geo-Reinforced Layered Sand", International Journal of Advanced Engineering Technology, Vol.2, No.2, pp.192-196.

[9] Rinaldi, R., (2012). "Inverted Shell Foundation Performance in Soil ", Ph.D. Thesis, Concordia University.

[10] Azzam, W.R., Nasr, A.M., (2015). Bearing capacity of shell strip footing on reinforced sand, Journal of Advanced Research, S2090-1232(14)00041-1.

[11] Al-Azzawi A., (2013). "A Study of the Behavior of Shell Footings using Finite Element Analysis", Eng. & Tech. Journal, Vol. 31, Part (A), No.19.

[12] Sajedi, K. et al., (2018). "Numerical and Experimental Comparisons of Different Behavior Shapes of Folded Plate Shell Foundation on Sandy Soil", Civil Engineering Sharif, Digital Identifier (DOI): 10.24200/ j30.2018.1334

[13] Sajedi, K. et al., (2019). "Elastic-Plastic Analysis of Inverted Folded Shell Strip Foundation on Sandy Soil", Journal of civil and environmental engineering, Article 2, Volume 47.4, Issue 89, Winter 2018, Page 15-26.

[14] Wood, D.M., (2004). "Geotechnical Modelling", E. & F.N. Spon Press, London.

[15] Jafarian, Y., Haddad, A., and Mehrzad, B., (2016). "Load settlement mechanism of shallow foundations rested on saturated sand with upward seepage", International Journal of Geomechanics, 17(3), pp. 1-14.

[16] Vargas-Monge, W., (1998). "Ring shear tests on large deformation of sand", Ph.D. thesis, University of Tokyo.

[17] Bishop, A.W., Green, G.E., Garga, V.K., Andresen, A. and Brown, J.D., (1971). "A new ring shear apparatus and its application to the measurement of residual strength", Geotechnique, 21(4), pp. 273-328.

[18] Abdollahi M. and Bolouri Bazaz J., (2017). "Reconstitution of Sand Specimens Using a Rainer System", International Journal of Engineering, Vol. 30, No. 10, pp. 1451-1463.

[19] Bolouri Bazaz J. and Mobinizad M. (2010). "Evaluation of the behaviour of Nahrein earth dam using finite element method and comparison with real magnitudes derived from instrumentation data", Journal of Iran water research (in Persian)", Vol. 4, No. 6, pp. 1-10.

[20] Yeganeh N., Bolouri Bazaz J. and Akhtarpour A. (2015). "Seismic analysis of the soil–structure interaction for a high rise building adjacent to deep excavation", Soil Dynamics and Earthquake Engineering. Vol. 79, pp. 149-170.